PCCP

Accepted Manuscript

ROYAL SOCIETY OF CHEMISTRY

www.rsc.org/pccp

PCCP

RSCPublishing

Single Molecule Confocal Fluorescence Lifetime Correlation Spectroscopy for Accurate Nanoparticle Size Determination

Bonghwan Chon, Kimberly Briggman and Jeeseong Hwang*

Cite this: DOI: 10.1039/x0xx00000x

Received 00th March 2014,
Accepted 00th June 2014

DOI: 10.1039/x0xx00000x

www.rsc.org/

We report on an experimental procedure in confocal single molecule fluorescence lifetime correlation spectroscopy (FLCS) to determine the range of excitation power and molecular or particulate concentration in solution under which the application of an unmodified model autocorrelation function is justified. This procedure enables fitting of the autocorrelation to an accurate model to measure diffusion length (r) and diffusion time (τ_D) of single molecules in solution. We also report on the pinhole size dependency of r and τ_D in a confocal FLCS platform. This procedure determines a set of experimental parameters with which the Stokes-Einstein (S-E) equation accurately measures the hydrodynamic radii of spherical nanoparticles, enabling the determination of the particle size range for which the hydrodynamic radius by the S-E equation measures the real particle radius.

Introduction

Unlike ensemble-averaged measurements of many particles, the characterization of physico-chemical properties of single nanoparticles (NPs) provides information on the detailed distribution of individual properties in the entire population. This information is essential to understanding and controlling the interaction of nanoparticles among themselves in engineering self-assembled structures[2], developing nanoparticle -based biological and chemical assays[3, 4], and assessing and controlling their influence on environmental, health, and safety interactions[5].

For imaging and characterization of individual NPs and molecules, electron microscopies such as scanning electron microscopy (SEM), transmission electron microscopy (TEM), scanning probe microscopies such as atomic force microscopy (AFM), and scanning tunnelling microscopy (STM) have been employed for structural analysis at nanometer and sub-nanometer spatial resolution[6-10]. A variety of analytical spectroscopy tools such as X-ray photoelectron spectroscopy, secondary ion mass spectroscopy, and nuclear magnetic resonance have also been instrumental to assess NP chemical compositions and structural details[11, 12]. However, the sensitivity of these techniques is limited to ensemble-averaged measurements, and samples need to be immobilized on a substrate or in a thin film for the measurement. On the other hand, optical measurements such as dynamic light scattering and fluorescence correlation spectroscopy (FCS) allow for the non-invasive assessment of the physico-chemical properties of single molecules and NPs in solution[13-17]. Platforms for single molecule FCS are confocal microscopy and total internal reflection microscopy[18, 19]. In confocal microscopy, single molecules in buffer solution or within a single cell diffuse through a focal volume of the excitation light, typically of sub-femtoliter volume[20]. In short, as a single molecule diffuses through the volume, a sensitive photon detector records the time trace of the fluorescence emission intensity from an individual dye molecule transiently existing in the volume. To ensure single molecule detection, the molecular concentration needs to be low enough that only a limited number of molecules exist in the solution so that one or no molecules are detected within the focal volume during a single time bin. On the other hand, the signal-to-noise ratio for photon detection has to be sufficient for a correlation function to be computed from the time-traced intensity fit to a physical model describing the molecule's dynamic physical properties in solution, such as local molecular concentration and hydrodynamic radius, and the diffusion time for a single particle in the confocal volume. In confocal detection, the autocorrelation function is calculated from the correlation of a time trace fluorescence intensity with itself shifted by time τ, and the physical model for the autocorrelation curve is described as the following function[21]:

$$G(\tau) = \frac{1}{V_{eff}\cdot\langle C\rangle}\cdot\frac{1}{1+\frac{\tau}{\tau_D}}\cdot\frac{1}{\sqrt{1+\left(\frac{r}{l}\right)^2\left(\frac{\tau}{\tau_D}\right)}}, \qquad (1)$$

where V_{eff} is an effective detection volume or confocal detection volume in a confocal microscope, and <C> is time-averaged concentration, τ_D is the lateral diffusion time, and *r* and *l* are the lateral and axial dimensions of the beam waist in the 3D Gaussian beam, respectively. Here, axial diffusion time τ_{Dz} is replaced with $(l/r)^2\tau_D$, assuming isotropic random diffusion. Note that *G(0)* or $1/\langle N\rangle$ is sometimes used instead of the pre-factor, $1/(V_{eff}\cdot\langle C\rangle)$. In the equation, the denominator of the first factor equals <*N*>, the time-averaged number of molecules in

the focal volume. Here, the confocal volume is approximated with the 3D Gaussian function which decays to $1/e^2$ at r in the lateral direction and l in the axial direction (z), and τ_D is the lateral diffusion time for which a molecule stays in the focal volume. The probability to detect a molecule within the effective volume is higher than $1/e^2$. The effective volume may be determined by different methods, and the accuracies of different methods are discussed elsewhere[22].

Recent studies have shown that dynamical properties of colloidal NPs and those of single molecules in solution are similarly described within certain ranges of measurement parameters and particle properties[23]. In essence, many of the optical analysis tools that have been used for single molecule characterization turned out to be applicable for the study of NPs with sizes comparable to those of organic fluorophores in solution. But great care needs to be taken when a single molecule measurement technique is applied to studies of both single NPs and single molecules. For measurement of nanoparticle size, the hydrodynamic radius is calculated from the Stokes-Einstein (S-E) equation by the following procedure. First, the computed autocorrelation function from the time-traced data is fitted to equation (1) to obtain the lateral diffusion time, τ_D. This value, along with the diffusion length, characterized by the beam waist (r *or* l), is used to calculate the diffusion coefficient (D) by

$$D = \frac{r^2}{4\tau_D} \qquad (2)$$

or

$$D = \frac{l^2}{4\tau_{Dz}}. \qquad (2)'$$

Second, the hydrodynamic radius value (R_h) of a spherical particle is determined from the S-E equation:

$$R_h = \frac{kT}{6\pi\eta D}, \qquad (3)$$

where k is the Boltzmann constant, T is the temperature (20 ℃ in this study), and η is the viscosity of the solvent (water in this study). Note that this S-E equation for spherical non-interacting particles undergoing Brownian motion is the dilute-solution approximation of the generalized S-E equation. Therefore, care needs to be taken when this is applied to non-spherical particles or highly concentrated samples. In a generalized S-E equation, the diffusion coefficient is corrected by a change of the viscosity due to changes in the effective viscosity of the solution as the particles may interact with each other. In addition, for compressible particles, the diffusion coefficient needs to be computed from the rate of osmotic-pressure change to the particle-volume change as the particles exhibit a swelling behaviour[24]. Quantitative characterization of such particles is challenging, as a rigorous model-based interpretation is required for the data, and the data must be collected under well-controlled experimental conditions. In this study, we focus on the size measurement of incompressible particles in a dilute limit to determine the optimized measurement conditions (laser power, particle concentration, and confocal pinhole size) and their size range, from which the S-E equation in a dilute limit provides realistic particle sizes without such complex corrections.

In summary, our approach allows for the determination of measurement conditions for proper modification to the model from which the experimental autocorrelation curve can be fit. Accordingly, r and τ_D at a specific pinhole size of the confocal microscope are accurately determined so that the S-E equation (3) is applied to measure the hydrodynamic radii of spherical NPs.

Experimental

We used an FCS setup based on an inverted confocal microscope (Leica, TCS SP5X) equipped with 60X oil-immersion objective (N.A 1.4, Leica). A schematic of our experimental setup and details are illustrated in Fig. 1. Samples were excited with 488 nm light selected from a super-continuum white light laser having a nominal repetition rate of 78.045 MHz, corresponding to 12.8 ns which was sufficiently longer than the fluorescence lifetime of Alexa 488 dyes which is measured to be 4.1 ns as shown in Figure S2 in the supplementary section. The broad continuous spectrum (super-continuum generation) is generated by propagating a pulsed laser light from a seed laser with the nominal wavelength of 1065.6 nm and nominal pulse width of 5 ps through a nonlinear photonic crystal fiber. The laser output selected by an installed acousto-optic tunable filter is 3.5 nm spectral band at 488 nm center wavelength. The instrument response function of time-correlated single photon counting (TCSPC) was estimated by the scattering signals of the excitation light using an avalanche photodiode detector (PDF-CTC, Micro Photon Device) and was measured to be 66 ps. This excitation light was focused on the samples by the objective. The fluorescence and scattered light were collected through the same objective and passed through the variable pinhole, which could be changed from 20 μm to 600 μm in diameter. The fluorescent signal was separated from the scattered laser light by a dichroic mirror (LPD01-488RU, Semrock) and band-pass filter (D525/50M, Chroma Technology), and focused onto a 62.5 μm multimode optical fiber, which acted as another pinhole for the rejection of potential ambient light, and was then coupled with the avalanche photodiode detector. For TCSPC measurements, the NIM output from the detector was connected to the input of a time-correlated single photon counter (TCSPC) analyser (PicoHarp 300, Picoquant) and detector router (PHR-800, Picoquant) for recording the time events, whereas the NIM output of the laser was also connected with the input trigger of TCSPC module. The instrument response of the entire system was about 66 ps (FWHM), providing 10 ps time resolution with deconvolution. This operated in the time-tagged time-resolved (TTTR) mode, which allowed recording the all-time events. Autocorrelation of the fluorescence bursts was obtained by these modules, and the autocorrelation curve was calculated and analysed using SymPho Time software (Picoquant).

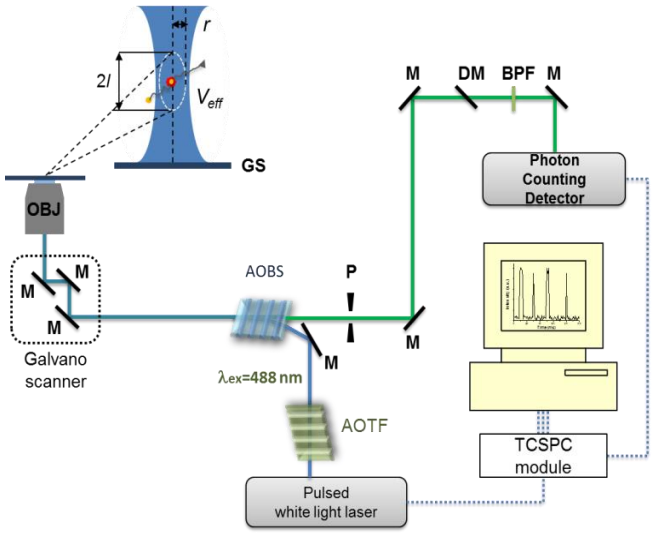

Fig. 1 A schematic of experimental setup and methods of FLCS. The FLCS setup is composed of: OBJ (objective lens with NA=1.4, Leica, Buffalo Grove, IL); M (mirror); DM (dichroic mirror with a cut-off wavelength of 488 nm); BPF (band-pass filter for 495 nm – 545 nm); P (adjustable pinhole); GS (No 1.5 glass substrate), AOBS (acousto-optical beam splitter); AOTF (acousto-optical tunable filter); *r* and *l* are the radial and axial beam waists at which the 3D Gaussian which decays to $1/e^2$.

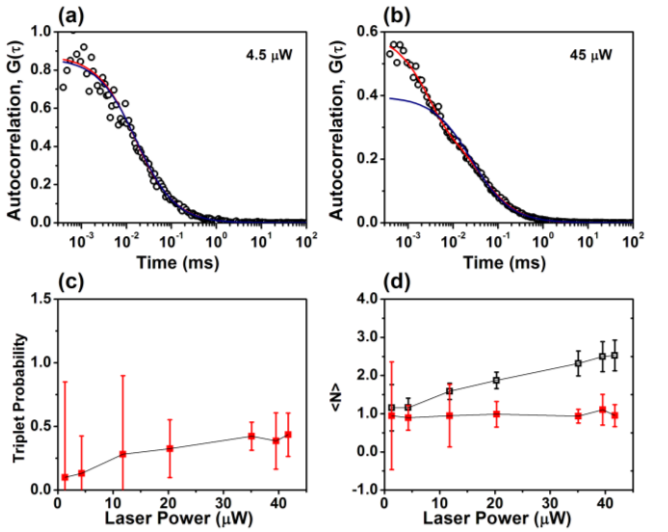

Fig. 2 Experimental autocorrelation functions of the Alexa 488 excited by two different excitation powers of (a) 4.5 μW and (b) 45.0 μW, respectively. The blue and red solid lines represent fits by a normal diffusion model (equation 1) or triplet-state-corrected diffusion model (equation 4), respectively. Plots are values of (c) the triplet probability and (d) the time-averaged molecule number as a function of the excitation power from the fits. Black and red are data points resulting from fits to the singlet model (equation 1) and triple-corrected model (equation 4), respectively.

Alexa Fluor 488 (A-20100, Invitrogen) diluted in ultrapure water (Barnstead Thermolyne, Dubuque, IA) for concentration-dependent measurements. To determine the exact concentration, the solution was measured by a UV-VIS spectrometer (Perkin-Elmer, Waltham, MA). Dragon green-labelled polystyrene fluorescent beads (Bangs Laboratories Inc., Fishers, IN) in 5% solid suspension (50 mg/mL) were used with nominal sizes of 50 nm, 100 nm, 190 nm, 310 nm, 520 nm, and 780 nm, and with nominal absorption and emission peaks at 480 nm and 520 nm, respectively. According to the manufacturer, the amount of dye equal to approximately 10-40% of the bead weight may be encapsulated within each bead [25]. The bead solutions were also diluted in the ultrapure water, followed by sonicating for 30 min for dispersion before the measurement.

For the FLCS measurements, the sample solution was contained in a 1 mm deep polydimethylsiloxane (PDMS) well on a No 1.5 glass coverslip with another No 1.5 glass coverslip covered on the top. The axial focal position was determined by a x-z confocal image and was maintained about 10 μm from the top surface of the bottom glass coverslip. The experiments were performed at 20 ℃ in a temperature-controlled laboratory with a fluctuation within 2 ℃ during measurements.

Results and discussion

A. Optimization of the excitation power

While a high laser-power excitation is desirable for better signal-to-noise ratios, optimization of the power is critical, as the increased power may result in non-radiative fluorescence decay processes that require modifications to the model autocorrelation function (1). However, under some experimental conditions such as the presence of reactive oxygen species or under high excitation power, a fraction of fluorescence decay processes involves decay via triplet states. Under these conditions, the fluorophores do not emit photons for a time period of τ_T, which is usually shorter than the diffusion time (τ_D) of interest and longer than the singlet decay time. In this circumstance the model autocorrelation function (1) is modified to the following

$$G_{Triplet}(\tau) = \left[1 - T + T \cdot e^{\left(-\tau/\tau_T\right)}\right] \cdot \frac{1}{V_{eff} \cdot \langle C \rangle} \cdot \sum_i F_i \cdot \frac{1}{1+\frac{\tau}{\tau_{D_i}}} \cdot \frac{1}{\sqrt{1+\left(\frac{r}{l}\right)^2\left(\frac{\tau}{\tau_{D_i}}\right)}}, \qquad (4)$$

where T is the fraction involving the triplet decay (0<T<1), τ_T is the corresponding lifetime involving triplet states, F_i are fractions of corresponding diffusion components, and τ_{Di} are diffusion times of corresponding diffusion components. The summation is introduced when the triplet decay may be sensitive to the local environment of the diffusion molecule. On the first order approximation, the solution is treated as a heterogeneous medium, and the summation is reduced to a single term only for i=1, where $F_1=1$ and $\tau_{Di}=\tau_D$ for fits to the experimental data. Measuring the fraction of triplet-state decay processes requires a time-correlated single photon counting (TCSPC) capability, as the differentiation between the singlet and triplet processes is done by comparing the light emission lifetimes for different processes[26]. To this end, a pulsed laser-based TCSPC technique

is integrated into a confocal FCS platform for fluorescence-lifetime correlation spectroscopy (FLCS)[27, 28]. In brief, two independent time samplings are performed and recorded for every photon detected. A macroscopic time stamp determines the duration of each time bin with respect to the beginning of the integration time for each time bin (~μs) as it is in the conventional continuous laser-based FCS technique. This contains the information related to the diffusion of fluorescent molecules or NPs and is used as in the conventional FCS technique. On the other hand, a microscopic time correlation records the short delay time (~ps) from the generation of each excitation laser pulse to the detection of each photon emitted by the fluorescence decay processes through either singlet or triplet states. These two independent timings enable us to measure the intensity time trace and fluorescence lifetimes of the fluorophores either in a single form or attached to the NP under investigation. Other advantages for TCSPC are in the effective rejection of scattering signals involving Rayleigh or Raman processes and detector-after-pulsing artifacts that would not exhibit measurable delays. The advantage of this FLCS approach is illustrated in Fig. S1 of the supplementary information.

Power-dependent reversible photobleaching or "blinking" of Alexa-488 molecules involves non-radiative dark states induced at high excitation power that lasts for a longer time than the detection bin time [29]. Therefore, the model autocorrelation equation (1) involves only radiative fluorescence decay (i.e. singlet) processes with negligible multi-photon effects [30-32]. The photons contributing to the fluorescence lifetimes are only radiative photons, therefore the lifetimes should remain the same regardless of the excitation intensity. This is demonstrated in the supplementary material, Figure S2. However, the existence of non-radiative or triplet decay processes requires modification of the model autocorrelation function of equation (1).

Since this triplet decay-involving term may increase the uncertainty in the fits, application of the unmodified model (equation 1) involving only a single fluorescence lifetime is desired for more accurate fits. The following procedure can determine the upper limit of the excitation power, under which the unmodified model can safely be applied. Fig. 2(a) and (b) exhibit typical autocorrelation data from 5.4 nM Alexa 488 fluorophores measured at several excitation powers between 2.0 μW and 45.0 μW. Here, 1.0 μW corresponds to approximately 0.704 kW/cm^2 focused onto a diffraction limited confocal spot of the 488 nm beam with a 1.4 NA oil immersion objective lens. The emission intensity at the maximum power, 45.0 μW, was ≤ 1 x 10^6 counts per second. This is still well below the detector's saturation limit of 11.8 x 10^6 counts per second, nullifying a concern about possible distortion in fitting the autocorrelation curve. For these measurements, a confocal pinhole size is fixed to 1 Airy, which corresponds to 97 μm in nominal diameter. The determination of precise diameters (in SI units) corresponding to Airy numbers requires precise calibration based on the measurements of the point spread function as a function of the pinhole size, and this is beyond the scope of current study. Under 4.5 μW, the experimental autocorrelation curves fit well to both the unmodified and modified model autocorrelation functions, since the fit to the modified model of equation (4) results in $T = 0$. However, as the power is increased above 4.5 μW, as shown in Fig. 2(b) for 45 μW excitation power, the experimental curve is not well fitted to the unmodified model (blue line) with a large chi-square value ($\chi^2 = 5.376$), but the modified model appears to provide a good fit for the experimental curve (for non-zero T, red line) with a much reduced chi-square value ($\chi^2 = 1.016$). Fig. 2(c) plots T values vs. excitation power, showing that the probability of triplet decay processes increases as the excitation power increases. At the excitation power of 30 μW or above, the triplet decay probability converges to about 0.44 and the estimated triplet lifetime in this regime is about 2.7 μs, which agrees well with the reported value elsewhere[33]. In defining the upper limit of the excitation power at or under which the unmodified autocorrelation is confidently applied, the large fitting errors in Fig. 2(c) make it difficult to determine the maximum laser power up to which T remains zero. Alternatively, Fig. 2(d) compares the number of time-averaged molecules obtained from two different fits (by equation (1) or (4)) of experimental autocorrelation curves measured at various excitation powers. Fitting errors in this plot are relatively smaller, allowing for the determination of the upper power limit. The time-averaged number of molecules consistently remains the same (≈1) for the entire laser power range when the fit is done using the modified autocorrelation model in equation (4). However, when the fit is forced to the unmodified model,

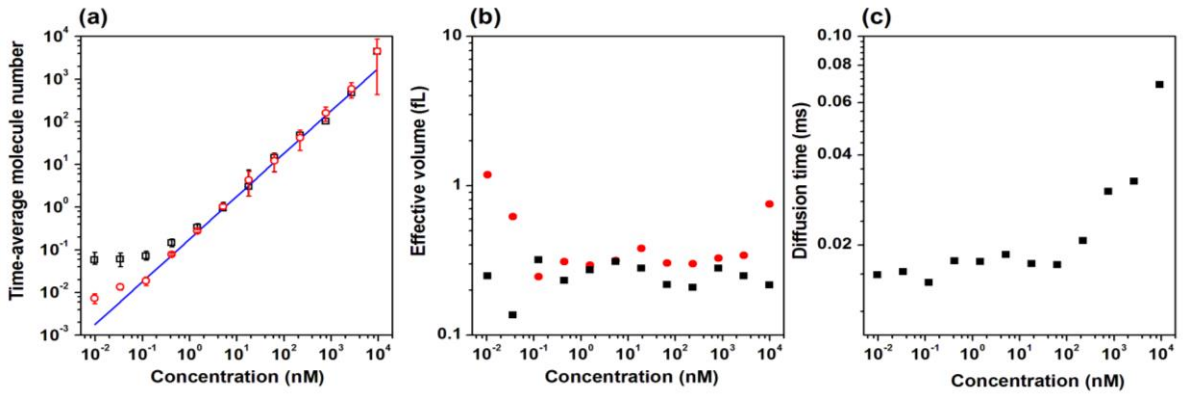

Fig. 3 Concentration dilution series measurements of Alexa 488 molecules in DI water. (a) Time-averaged molecule number vs. concentration. The black squares are raw data and the red circles are for data after background correction. (b) Fitted values of effective volume vs. molecule concentrations. (c) Fitted diffusion time values vs. molecule concentrations. The errors of both (b) and (c) are smaller than their symbols.

equation (1), the numbers are overestimated. With the power at 4.5 μW or less, the numbers obtained from two fits are similar within the fit errors; therefore, we set 4.5 μW as the upper limit of the excitation power below which the unmodified autocorrelation fit to equation (1) can be used appropriately.

B. Optimization of the particle concentration

Because the S-E equation (3) holds for the dilute limit, the concentration of particles in solution needs to be limited to one molecule in the detection volume. As discussed in the previous section, with 5.4 nM Alexa 488 molecules in water, about one molecule is estimated in the detection volume, which is defined by both the diffraction-limited focal volume of the laser beam and the confocal pinhole size. However, at or below this limit, the signal-to-noise ratio may not be sufficient, since shot noise for a long period of time will dominate over rare fluorescence emission events from a single molecule or single particle, necessitating a correction for the background noise. Fig.s 3(a) and (b) present the results of the number of molecules and the diffusion time from fits of the experimental data to the unmodified autocorrelation model of equation (1). To assure that the triplet decay probability is negligible, the excitation power was maintained at 4.5 μW for all the measurements. Fig. 3(a) shows the molecule numbers $\langle N\rangle = 1/G_o$ present in the effective detection volume fit using equation (1) at different sample concentrations (black data points). Below 1 nM concentrations, the fits overestimate the numbers compared to the actual numbers by independent UV-VIS measurements. In this regime, the uncorrelated background noise is dominant, and needs to be corrected by $\langle N\rangle = 1/\chi^2 G_o$, where the correction factor $\chi^2 = [1 + \langle b\rangle/(\langle F\rangle - \langle b\rangle)]^2$. Here, $\langle b\rangle$ is the averaged background count rate measured on a sample containing only solvent, and $\langle F\rangle$ is the actual measured count rate of the solution with fluorophores included; then $(\langle F\rangle - \langle b\rangle)$ is the virtual count rate with no background contribution[34]. After this background correction, the number of molecules vs. concentration exhibits a linear relation that agrees well with the UV-VIS results. This linear fit to the corrected data points (red dots) estimates ≈0.35 fL for the detection volume. However, the post-correction data points for the concentrations below 1 nM still deviate from the linear fit, implying that the residual background signal may still remain in this regime. To apply the S-E equation for size measurements, the confocal volume or effective detection volume needs to be precisely calculated from the fits; the diffusion length, *r* in equation (2) is calculated from this volume. To test the reliability of the data points in calculating the diffusion length, effective volumes at various concentrations of single molecules are calculated by $V_{eff} = \langle N\rangle/N_a c$, where <*N*> is the time-averaged molecule number shown in Fig. 3(a), and the result is displayed in Fig. 3(b), where concentration is from the independent UV-VIS results, and *Na* is Avogadro's number. For these measurements, we used only single molecules not nanoparticles due to a concern that the diffusion time may be prolonged as the size of particle is not negligible to the beam waist, i.e. fluorescence emission may still be collected by the detector even after the center of mass of the nanoparticle is translated out of the beam waist resulting in overestimation of the effective volume. Fig. 3(c) also exhibits that the diffusion time is significantly increased at high molecular concentrations indicative of collision of molecules under a high population condition. Effective volumes for concentrations above 1 nM are approximately the same (0.3 fL) which agrees well with the volume estimated from the linear fit in Fig. 3(a). However, the calculated effective volume below 1 nM significantly fluctuates.

C. Pinhole size-dependent diffusion length and time

In a dilute concentration regime, the S-E equation (4) is used to calculate the hydrodynamic radius of spherical particles. The diffusion length, *r*, used to obtain the diffusion coefficient (*D*) in equation (3) is estimated by inserting the known values of (*r/l*), *G(0)* and <*C*> into the following equation:

$$r = \frac{1}{\sqrt{\pi}}\left[\left(\frac{r}{l}\right)\cdot V_{eff}\right]^{\frac{1}{3}} = \frac{1}{\sqrt{\pi}}\left[\left(\frac{r}{l}\right)\cdot\frac{1}{G(0)\langle C\rangle}\right]^{\frac{1}{3}}. \quad (5)$$

Here, the effective volume, $V_{eff} = \pi^{1.5} r^2 l$, is used for the diffraction-limited 3D Gaussian focal volume of a confocal beam with $1/e^2$ beam waists (diameters) of *r* and *l* in the lateral and axial direction, respectively. To calculate *r*, the *G(0)* value obtained from the autocorrelation fit and <*C*> from independent UV-VIS spectroscopy measurements were used. Note that the initial *r* and *l* are for a diffraction-limited confocal spot and

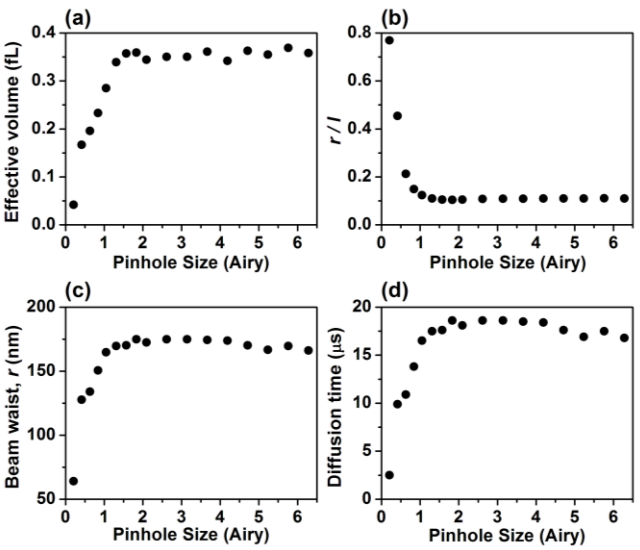

Fig. 4 Pinhole-size dependence of the effective volume (a), the ratio of the radial and lateral beam waists , *r/l* (b), radial beam waist, *r* (c), and the diffusion time (d) of Alexa 488 fluorophores in DI water. The "Airy," not a SI unit, is used for the size of the confocal pinhole in this report. The determination of real diameters (in SI units) corresponding to Airy numbers needs precise calibration based on the measurements of the point spread function as a function of the pinhole size, and is beyond the scope of the current study.

depend only on numerical aperture and the wavelength of the light. These values are initially independent of the confocal pinhole size, since the confocal pinhole is located in the detection path. However, the effective detection volume depends on the confocal pinhole size and is quantified by the Airy number of a tightly focused beam. The Airy pattern is the description of the diffraction-limited focused spot with a perfect lens through a circular aperture and is composed of a bright spot, a so-called Airy disc, at the center, and a series of concentric peripheral alternating bright and dark rings with diminishing intensity and contrast away from the center[35]. In a confocal detection, when the pinhole size is set to << 1 Airy, where 1 Airy corresponds to the diameter of an Airy disc defined by a radial distance between first two minima in the Airy pattern, the collected light is significantly diffracted, resulting in a substantially reduced far-field intensity, with most of the photons confined in the near-field to the pinhole. On the other hand, as the pinhole size increases to 1 Airy and beyond, the effective volume converges to a diffraction-limited focal volume of ≈0.35 fL as shown in Fig. 4(a). This value for the effective volume agrees well with the result deduced from Fig. 3(a). For these measurements, 5.12 nM concentration was used with excitation power fixed at 4.5 μW, as these parameters were determined by the optimization procedure discussed in previous sections. The pinhole size-dependent (*r/l*) values at various Airy numbers are from the autocorrelation fits and are plotted in Fig. 4(b). The converging value of ≈0.1 of the ratio, *r/l*, for pinhole sizes > 1 Airy estimates the aspect ratio of a diffraction-limited 3D confocal spot. This aspect ratio is about one third as large as a theoretically estimated value for a diffraction limited focal volume[36,35]:

$$\frac{FWHM_{radial}}{FWHM_{axial}} = \frac{\frac{0.51\lambda}{NA}}{\frac{0.88\lambda}{n-\sqrt{n^2-NA^2}}} \approx 0.37. \qquad (6)$$

Considering the index mismatch at the water-glass interface at the top surface of the glass substrate and aberrations of the objective lens, a difference of a factor of three is not surprising. After using V_{eff} and (*r/l*) in equation (5), Fig. 4(c) shows that the diffusion length at the diffraction-limit regime agrees well with the lateral resolution of the confocal microscopy at the wavelength used, indicating that (*r/l*) and V_{eff} synergistically appear to reduce the overall fitting error, as these two parameters are coupled and simultaneously change as the pinhole size varies. Finally, diffusion times for different pinhole sizes are also obtained from the autocorrelation fits and are displayed in Fig. 4(d). The procedure in this section suggests that precise determination of the r and τ_D values requires the plot of these values against pinhole sizes from which r and τ_D values need to be determined at a specific pinhole size used in the confocal setup.

D. Nanoparticle size measurements

Previous sections provide a sound groundwork for determining the range of important experimental parameters in confocal single molecule FLCS and conditions under which the unmodified autocorrelation model may appropriately be used for fitting experimental autocorrelation curves. The TCSPC technique was necessary on the fluorescence beads to differentiate the emission involving singlet decays from the triplet decays. Based on the procedure, as long as the excitation power is maintained at less than 4.5 μW and the bead concentration between 1 nM and 100 nM, we can precisely determine diffusion length and diffusion time at a given confocal pinhole size by fitting experimental autocorrelation functions to an unmodified model, equation (1). The model autocorrelation equation (1) may need to be modified if the laser intensity of 4.5 μW in nanoparticle measurements induces triplet state decays in dragon green dyes. The same would be true if inter-particle collisions in 1 nM concentration were noticeable. However, under 1 Airy pinhole size with small nanoparticles, the

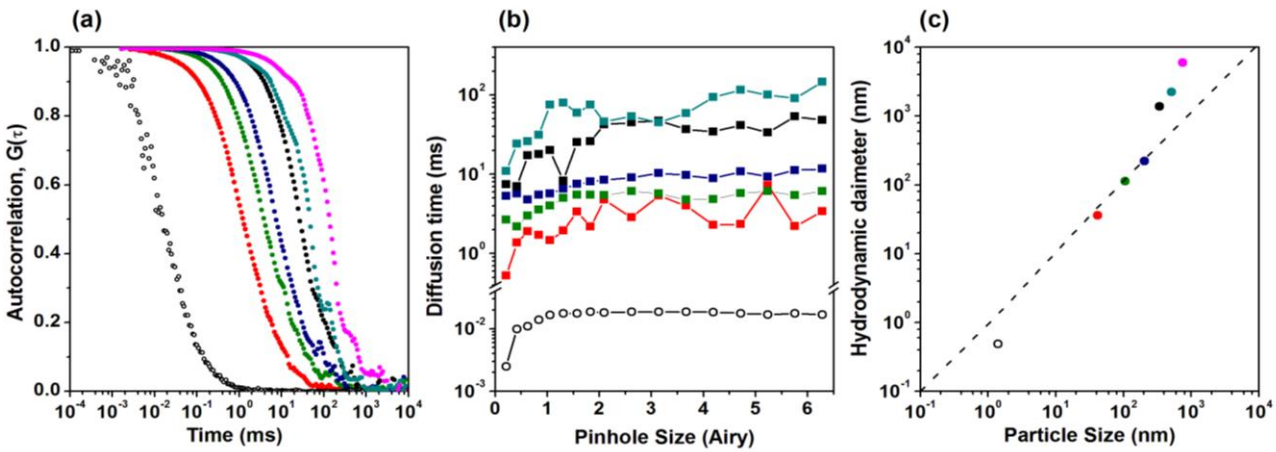

Fig. 5 (a) Autocorrelation curves of Alexa 488 molecules (black circles) and of 6 different-sized fluorescent beads. Measured bead diameters by SEM are 41.4 nm ± 6.8 nm (red), 106.2 nm ± 1.3 nm (green), 205.6 nm ± 9.0 nm (blue), 340.2 nm ± 3.2 nm (black), 513.4 ± 2.9 nm (aqua), and 749.3 ± 4.8 nm (magenta). The diameter of the Alexa 488 molecule is estimated to be 1.4 nm by the S-E equation, assuming a spherical shape. (b) The pinhole-size dependent diffusion times from autocorrelation fittings of single molecule and NP data. (c) A plot of particle size diameters of the Alexa 488 molecule assuming the spherical shape[1] and fluorescent beads by SEM measurements vs. hydrodynamic diameter obtained by FLCS measurements and the S-E equation.

autocorrelation data were fit well with equation (1), suggesting that no further modification to the equation (1) is necessary. For the size analyses of fluorescent NPs, the above procedures of FLCS developed for single molecules are also applied. Time traces of fluorescence intensities for NPs of different sizes were collected under the optimized conditions discussed above. From these, autocorrelation curves are obtained as shown in Fig. 5(a), where the size-dependent decay is clearly shown; larger particles exhibit a slower decay. In the same plot, an autocorrelation curve of single Alexa 488 molecules is displayed to compare much faster decays than any NP case. The diffusion times from fits of autocorrelation curves to the model confirms that the larger the NP size, the slower is the diffusion, as shown in Fig. 5(b). In addition, note that the diffusion time increases as the pinhole size increases, indicative of the increase in the detection volume. From these plots, the diffusion times for each particle at 1 Airy unit are obtained.

Finally, the diffusion length and diffusion time obtained by the procedure described above are used to calculate the hydrodynamic radii of NPs in the S-E equation (3), and the result is shown in Fig. 5(c) along with the average particle diameter directly measured from the corresponding SEM images of NPs for each size (see SEM images in Figure S3 of the supplementary information). For single molecules, the 1.4 nm size of Alexa 488, assuming its spherical shape[1], was used to compare our measurement using the S-E equation. Note that particle sizes of 41.4 nm ± 6.8 nm, 106.2 nm ± 1.3 nm, and 205.6 nm ± 9.0 nm by the FLCS-based S-E equation are the same as the measurements determined by SEM within the measurement error. For these sizes, the FLCS-based technique precisely measures the real NP sizes. However, for larger particles, our technique consistently overestimates the size as expected; the diffusion time is prolonged as the size of particle increases to a size comparable to or larger than the beam waist. In this regime, fluorescence emission is still collected by the detector even after the center of mass of the bead is translated out of the beam waist, resulting in overestimation of the particle size. For quantitative discussion on this aspect, we are currently investigating the size- and position-dependent point spread function convolution effect in confocal microscopy of nanoparticles.

The fluorescently labelled beads have multiple fluorophores as the fluorescence emission from single beads is definitely higher than that of single fluorophores and noticeable "blinking" in the fluorescence emission is not observed in the beads at low power excitation. In this study, the distribution of fluorophores is assumed to be uniform within the bead, based on the manufacturer's synthesis protocol. The effect of multiple fluorophores, regarding particle geometry and their intra-particle distribution is substantially discussed elsewhere[37]. According to this report, the fluorophore distribution affects the shape of the autocorrelation function for a surface- and internally-labelled sphere of equal diameter. However their findings indicate that, for sub-micrometer size particles with the same size, this difference is not sufficient to distinguish particles with different fluorophore distributions.

Conclusions

In summary, we report an experimental procedure for determining the ranges of excitation power and concentration in confocal single molecule FLCS for which the unmodified autocorrelation model may appropriately be applied to fit experimental autocorrelation curves. We also demonstrate that diffusion length and diffusion time are dependent upon the confocal pinhole size. These findings allow for fitting the autocorrelation to a proper model to accurately measure diffusion lengths and diffusion times of single molecules and single nanoparticles in confocal excitation volumes so that the Stokes-Einstein equation is applied to accurately measure the hydrodynamic radii of spherical nanoparticles. Our results show the FLCS-based S-E equation provides the accurate sizes of nanoparticles in the size range from 41.4 nm ± 6.8 nm to 205.6 nm ± 9.0 nm. This study provides a solid groundwork for the development of standardized experimental protocols in applying the S-E equation for accurate NP size measurement.

Acknowledgements

This research was supported by the NIST intramural innovative measurement science (IMS) program on "optical medical imaging for clinical applications" and by the NIST intramural NanoEHS program. The authors thank Dr. Minhua Zhao for SEM imaging of NPs. The authors also thank Drs. David Allen, Maritoni Litorja, Eric Shirley, Vivek Prabhu, and Ajit Jillavenkatesa at NIST for useful discussions. Certain commercial equipment, instruments, or materials are identified in this manuscript to foster understanding. Such identification does not imply recommendation or endorsement by the National Institute of Standards and Technology, nor does it imply that the materials or equipment identified are necessarily the best available for the purpose.

Notes and references

Quantum Electronics and Photonics Division, Physical Measurement Laboratory, National Institute of Standards and Technology, 325 Broadway, Boulder, CO 80305, USA
Email: jch@nist.gov

†Electronic Supplementary Information (ESI) available: Advantage of the FLCS measurement, laser excitation power-dependent fluorescence lifetimes of Alexa 488 dyes, and SEM images of the beads. See DOI: 10.1039/b000000x/

References

1. A. Masuda, K. Ushida and T. O. Riken, *Biophysical Journal*, 2005, **88**, 3584-3591.
2. G. M. Whitesides, J. P. Mathias and C. T. Seto, *Science*, 1991, **254**, 1312-1319.
3. M. E. Akerman, W. C. W. Chan, P. Laakkonen, S. N. Bhatia and E. Ruoslahti, *Proceedings of the National Academy of Sciences of the United States of America*, 2002, **99**, 12617-12621.
4. M. Howarth, W. H. Liu, S. Puthenveetil, Y. Zheng, L. F. Marshall, M. M. Schmidt, K. D. Wittrup, M. G. Bawendi and A. Y. Ting, *Nature Methods*, 2008, **5**, 397-399.

5. E. Subcommittee on Nanoscale Science, and Technology National Nanetechnology, C. o. Technology and N. S. a. T. Council, *Strategy for nanotechnology-related environmental, health, and safety research*, National Nanotechnology Coordination Office, Arlington, VA2008.
6. S. P. Ahrenkiel, P. R. Yu, J. E. Murphy, J. M. Nedeljkovic and B. S. Donohoe, *Journal of Microscopy*, 2008, **230**, 382-387.
7. Z. L. Wang, *Advanced Materials*, 1998, **10**, 13.
8. A. Rao, M. Schoenenberger, E. Gnecco, T. Glatzel, E. Meyer, D. Brandlin and L. Scandella, *Proceedings of the International Conference on Nanoscience and Technology*, 2007, **61**, 971-976.
9. X. Liu, M. Yu, H. Kim, M. Mameli and F. Stellacci, *Nature Communications*, 2012, **3**, 1182.
10. A. M. Jackson, Y. Hu, P. J. Silva and F. Stellacci, *Journal of the American Chemical Society*, 2006, **128**, 11135-11149.
11. M. Fuchs, D. Breitenstein, M. Fartmann, T. Grehl, S. Kayser, R. Koester, R. Ochs, S. Schlabach, D. V. Szabo and M. Bruns, *Surface and Interface Analysis*, 2010, **42**, 1131-1134.
12. L. J. Chen, S. S. Shah, J. Silangcruz, M. J. Eller, S. V. Verkhoturov, A. Revzin and E. A. Schweikert, *International Journal of Mass Spectrometry*, 2011, **303**, 97-102.
13. R. BarZiv, A. Meller, T. Tlusty, E. Moses, J. Stavans and S. A. Safran, *Physical Review Letters*, 1997, **78**, 154-157.
14. R. Pecora, *Journal of Nanoparticle Research*, 2000, **2**, 123-131.
15. D. Magde, W. W. Webb and E. Elson, *Physical Review Letters*, 1972, **29**, 705-708.
16. M. Eigen and R. Rigler, *Proceedings of the National Academy of Sciences of the United States of America*, 1994, **91**, 5740-5747.
17. R. Rigler, *Journal of Biotechnology*, 1995, **41**, 177-186.
18. K. Bacia, S. A. Kim and P. Schwille, *Nature Methods*, 2006, **3**, 83-89.
19. N. L. Thompson and B. L. Steele, *Nature Protocols*, 2007, **2**, 878-890.
20. R. Rigler, U. Mets, J. Widengren and P. Kask, *European Biophysics Journal with Biophysics Letters*, 1993, **22**, 169-175.
21. E. L. Elson and D. Magde, *Biopolymers*, 1974, **13**, 1-27.
22. S. Ruttinger, V. Buschmann, B. Kramer, R. Erdmann, R. Macdonald and F. Koberling, *Journal of Microscopy*, 2008, **232**, 343-352.
23. H. Liao, L. Cui, S. Whitelam and H. Zheng, *Science*, 2012, **336**, 1011-1014.
24. A. L. Kholodenko and J. F. Douglas, *Physical Review E*, 1995, **51**, 1081-1090.
25. R. Arshady, *Biomaterials*, 1993, **14**, 5-15.
26. D. V. O'Connor and D. Phillips, *Time-Correlated Single Photon Counting*, Academic P1984.
27. M. Bohmer, M. Wahl, H. Rahn, R. Erdmann and J. Enderlein, *Chemical Physics Letters*, 2002, **353**, 439-445.
28. S. Ruttinger, P. Kapusta, M. Patting, M. Wahl and R. Macdonald, *Journal of Fluorescence*, 2010, **20**, 105-114.
29. D. Baddeley, I. D. Jayasinghe, C. Cremer, M. B. Cannell and C. Soeller, *Biophysical Journal*, 2009, **96**, L22-L24.
30. P. S. Dittrich and P. Schwille, *Applied Physics B-Lasers and Optics*, 2001, **73**, 829-837.
31. C. Eggeling, A. Volkmer and C. A. M. Seidel, *Chemphyschem*, 2005, **6**, 791-804.
32. V. Iyer, M. J. Rossow and M. N. Waxham, *Journal of the Optical Society of America B-Optical Physics*, 2006, **23**, 1420-1433.
33. S. T. Hess, S. H. Huang, A. A. Heikal and W. W. Webb, *Biochemistry-Us*, 2002, **41**, 697-705.
34. S. T. Hess and W. W. Webb, *Biophysical Journal*, 2002, **83**, 2300-2317.
35. H. Beyer, *Handbuch der Mikroskopie*1985.
36. S. Wilhelm, B. Gröbler, M. Gluch and H. Heinz, 1997.
37. B. Wu, Y. Chen and J. D. Muller, *Biophysical Journal*, 2008, **94**, 2800-2808.

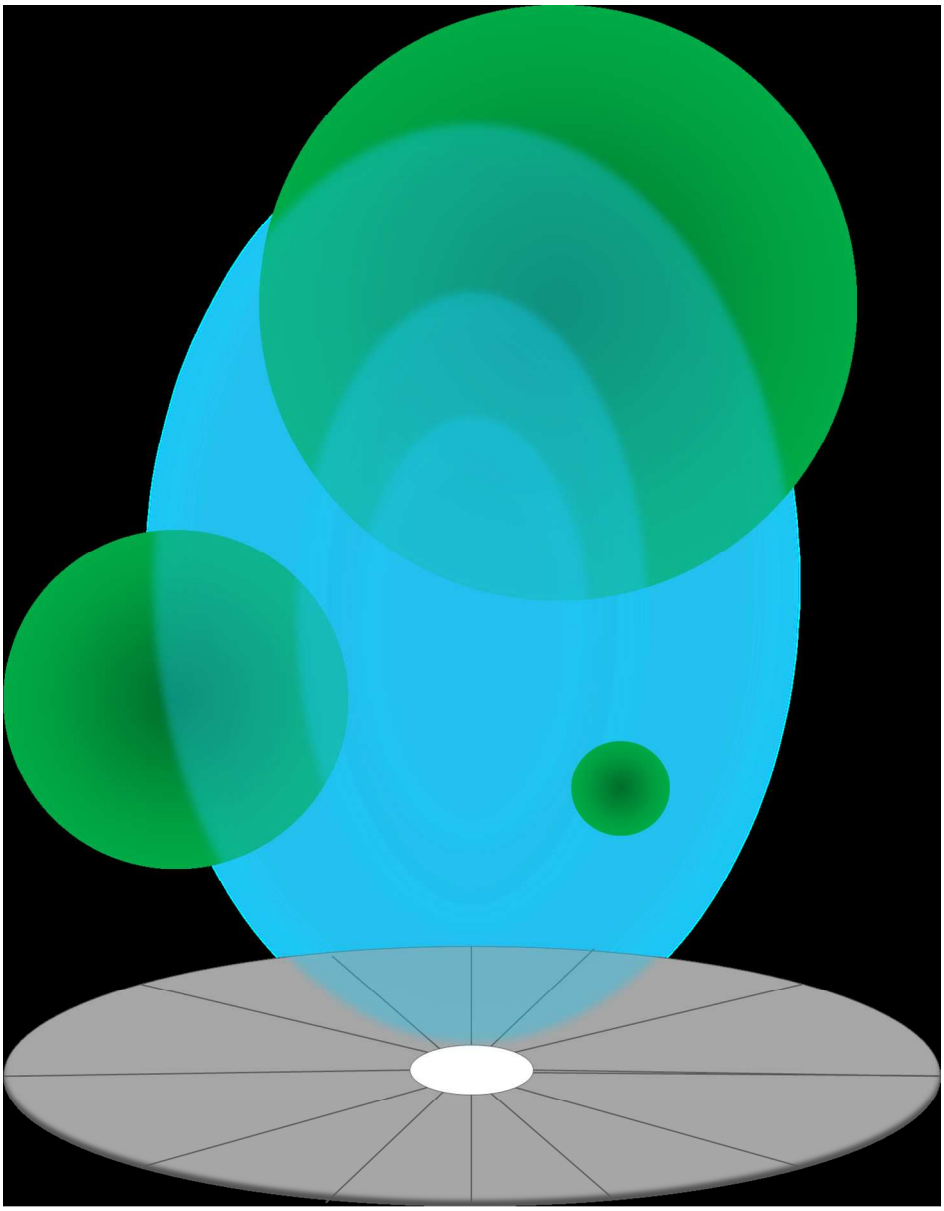

241x309mm (150 x 150 DPI)